ViT-SpSH: A Hybrid Transformer-Spectral Head Architecture for Chromatic Aberration Detection and Localization

Jarosław Bernacki[1][0000−0002−4488−3488]
Rafał Scherer[2,3][0000−0001−9592−262X]

[1] Department of Computer Science and Systems Engineering
Wrocław University of Science and Technology
Wybrzeze Wyspiańskiego 27
50-370 Wrocław, Poland
jaroslaw.bernacki@pwr.edu.pl
[2] Department of Artificial Intelligence, Faculty of Computer Science and Artificial Intelligence
Częstochowa University of Technology
al. Armii Krajowej 36, 42-200 Częstochowa, Poland
[3] Faculty of Computer Science
and Center of Excellence in Artificial Intelligence, AGH University of Krakow
al. Mickiewicza 30, 30-059 Kraków, Poland
rafal.scherer@pcz.pl

Abstract. Chromatic aberration remains a common optical artifact in digital photography, manifesting as color fringing along high-contrast edges due to wavelength-dependent lens refraction. This paper proposes a hybrid vision transformer-based architecture for the accurate detection and localization of chromatic aberration in single RGB images. The method employs a pretrained ViT encoder to extract global contextual patch embeddings capturing long-range spatial dependencies. In parallel, chromatic residual maps are computed from inter-channel differences to explicitly highlight spectral misalignments. These residuals are fused early with ViT embeddings, followed by cross-attention refinement and convolutional upsampling in a dedicated spectral segmentation head, yielding a high-resolution probability map of aberration regions. Experiments on a diverse dataset of real-world photographs demonstrate that the proposed hybrid approach significantly outperforms classical convolutional baselines (classic CNN, U-Net, FCN-VGG) in classification accuracy, offering a robust tool for automated optical quality assessment.

Keywords: image processing · chromatic aberration · vision transformer · deep learning

1 Introduction

Digital forensics is a branch of forensic science focused on the identification, acquisition, analysis, and preservation of digital evidence in a manner that is

ICCS Camera Ready Version 2026
To cite this paper please use the final published version:
DOI: 10.1007/978-3-032-29909-3_30

legally acceptable. It deals with data stored, processed, or transmitted by digital devices and systems, ensuring that such information can be reliably used in investigations and court proceedings. The field covers a wide range of areas, including computer forensics (analysis of personal computers and servers), mobile device forensics (smartphones and tablets), network forensics (monitoring and analysis of network traffic), multimedia forensics (authentication and analysis of images, audio, and video), and cloud forensics (investigation of data stored in cloud environments). Digital forensics is applied both in criminal investigations and also in civil litigation, incident response, cybersecurity, and corporate investigations, making it possible to uncover digital traces of human activity [7].

The scope of digital forensics also includes the analysis of optical artifacts present in digital images, such as vignetting [10], geometric distortion [2, 24], chromatic aberrations [18, 8], and other lens- or sensor-related imperfections [9, 16]. These defects arise from the physical properties of imaging systems and often exhibit device-specific characteristics, making them valuable forensic cues. Examining such optical traces enables digital forensics to be usable in tasks such as source camera identification [17, 1], image authenticity verification [31], and detection of tampering or manipulation [21, 13].

Chromatic aberration (CA) is an optical artifact arising from the wavelength-dependent refraction of light in lens systems, causing different colors (red, green, and blue channels in digital imaging) to focus at slightly different points. This results in color fringing, typically purple or green halos, along high-contrast edges, where channel misalignments become visible. The defect manifests in two main forms: axial (longitudinal) chromatic aberration, producing color-dependent blur along the optical axis due to varying focal planes [4], and lateral (transverse) chromatic aberration, generating radially increasing color shifts that are most pronounced toward the image periphery [6]. In real-world photography, these distortions are particularly evident in scenes with bright objects against dark backgrounds or sharp transitions, degrading overall image quality and posing challenges for computational correction and analysis [25].

In this paper, we propose a hybrid architecture ViT-SpSH that combines the vision transformer (ViT) with a specialized spectral segmentation head (SpSH) for accurate detection and localization of lateral chromatic aberration (LCA) in photographic images. The method processes the input RGB image through a pretrained ViT encoder, which divides the image into patches and extracts global contextual embeddings via multi-head self-attention and feed-forward layers. In parallel, chromatic residual maps are computed from inter-channel differences to highlight spectral misalignments. These residuals are fused early with ViT embeddings, followed by cross-attention refinement and convolutional upsampling in the spectral segmentation head, producing a precise probability map of aberration regions. This hybrid design effectively integrates long-range spatial context with explicit spectral sensitivity, enabling reliable performance in identifying subtle color fringes compared to purely convolutional or standard transformer-based approaches. The experimental evaluation of the ViT-SpSH

ICCS Camera Ready Version 2026
To cite this paper please use the final published version:
DOI: 10.1007/978-3-032-29909-3_30

method over several baseline models confirmed the CA identification accuracy in terms of accuracy, precision, recall, and F_1 measures.

Organization of the paper The paper is organized as follows. Section 2 discusses the previous and related work. In section 3 we describe the proposed method. In section 4, the experimental evaluation results are presented. The final section concludes this work. Everywhere in the paper, bold face denotes matrices or vectors.

2 Previous and related work

The work in [30] introduces a two-stage multi-task learning framework designed to detect CA in ceramic tiles. The approach integrates deep multi-task feature extraction, capturing texture and global color information, with handcrafted color statistics. The resulting discriminative descriptor is then used to train a multilayer perceptron classifier. Experimental validation on real-world datasets confirms both high detection accuracy and computational efficiency.

The study in [23] investigates the transferability of CA calibration between different cameras sharing the same lens. In [19, 20], lateral chromatic aberration is modeled for copy–paste forgery detection using a hypothesis testing framework based on discrepancies between local and global LCA estimates. Additional works on CA correction and analysis are reviewed in [5, 14, 22, 27, 26, 28]. Chromatic aberration has also been used as a cue for image authenticity. In [29], CA-related artifacts are exploited to detect image forgeries, leveraging their sensitivity to manipulation and difficulty of replication. The work in [15] addresses CA in hyperspectral imaging, proposing a correction method based on spectral measurements and dispersion compensation.

3 The proposed method

The proposed hybrid architecture for CA detection integrates two processing branches to utilize both global contextual understanding and spectral-specific cues, ultimately fusing them to generate a high-resolution per-pixel probability map. This design draws on the strengths of transformer-based models for scene-wide dependencies while using lightweight spectral analysis tailored to the unique characteristics of CA, such as color fringing on high-contrast edges. The first branch employs a pretrained vision transformer (ViT) encoder for extracting hierarchical representations from images. Specifically, the input RGB image is partitioned into non-overlapping patches (16×16 pixels), each of which is linearly projected into a fixed-dimensional embedding space to form a sequence of patch tokens. Then, these embeddings are augmented with learnable positional encodings to preserve spatial relationships, ensuring that the model can discern relative positions through the image. The sequence subsequently flows through a stack of 12 transformer layers, where each layer consists of a

ICCS Camera Ready Version 2026
To cite this paper please use the final published version:
DOI: 10.1007/978-3-032-29909-3_30

multi-head self-attention mechanism to capture long-range dependencies and intricate interactions between distant patches, followed by a feed-forward network (comprising two linear projections with a GELU activation) for non-linear feature transformation. Layer normalization and residual connections are applied to stabilize training. The output of this encoder is a set of refined ViT patch embeddings, which encapsulate global scene structure, semantic hierarchies, and salient high-contrast regions prone to chromatic fringes, providing a semantically rich foundation for downstream fusion.

The second branch constitutes the spectral segmentation head (SpSH), which is a specialized module that initiates processing with the direct computation of chromatic residual maps from the input RGB channels. These maps are generated as pairwise absolute differences $|\mathbf{R} - \mathbf{G}|$, $|\mathbf{G} - \mathbf{B}|$, and $|\mathbf{R} - \mathbf{B}|$, which effectively highlight pixel-wise discrepancies between color channels, isolating the purple-green or red-blue shifts emblematic of CA without relying on learned parameters. An early feature fusion mechanism is introduced at the entry point of the SpSH, which involves upsampling the ViT patch embeddings via bilinear interpolation to align with the full-resolution residual maps, followed by channel-wise concatenation to combine the representations dimensionally. Then, a subsequent 3×3 convolutional layer performs initial spatial integration, convolving over the concatenated features to smooth artifacts from the upsampling. A cross-attention fusion module further refines the features derived directly from the concatenated inputs. Employing multi-head attention (8 heads, each processing a subspace of the features), this module enables dynamic weighting of spectral discrepancies against global spatial cues. This allows treating residual maps as queries to attend to relevant ViT-derived keys and values and then enhancing alignment between local color anomalies and broader scene semantics while suppressing irrelevant noise.

The refined features from the cross-attention module are then channeled into a lightweight convolutional decoder, which progressively restores full spatial resolution through a series of three convolution layers (each consisting of 128 filters with 5×5 kernels and stride 2), interspersed with optional batch normalization and ReLU activations to maintain gradient flow and feature diversity. This decoder both upscales the patch-level abstractions back to pixel-level granularity and also preserves the intertwined spectral and contextual cues, ensuring that localized CA signals are not diluted during reconstruction. A final 1×1 convolutional layer reduces the multi-channel feature map to a single output channel, followed by a sigmoid activation to yield the dense CA probability map, where values range from 0 (no CA) to 1 (strong CA). This hybrid formulation allows for precise localization of chromatic fringes, even in complex scenes with varying lighting and textures, while inherently promoting robustness to diverse content through global attention.

The overall structure of the proposed hybrid approach, illustrating the parallel branches and fusion pathways, is depicted in Fig. 1.

ICCS Camera Ready Version 2026
To cite this paper please use the final published version:
DOI: 10.1007/978-3-032-29909-3_30

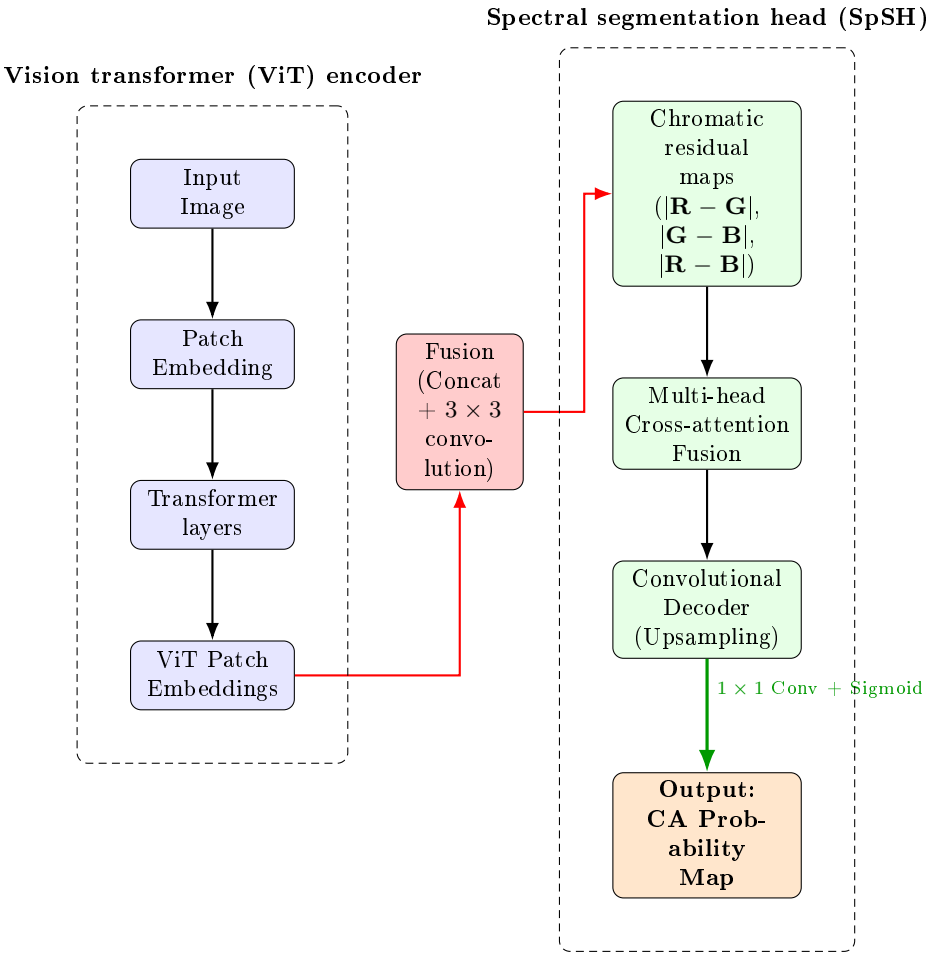

Fig. 1. Schematic of the proposed hybrid architecture.

3.1 Preliminaries and problem formulation

Chromatic aberration model As mentioned before, chromatic aberration arises from the wavelength-dependent refraction in optical lenses, where different colors (corresponding to red, green, and blue channels in digital imaging) focus at slightly different points. The observed image can be modeled as a superposition of channel-specific shifts:

$$\begin{aligned} \mathrm{CA}(x,y) = {} & I(x + d_x(\lambda_r), y + d_y(\lambda_r)) \cdot R \\ & + I(x + d_x(\lambda_g), y + d_y(\lambda_g)) \cdot G \\ & + I(x + d_x(\lambda_b), y + d_y(\lambda_b)) \cdot B, \end{aligned} \tag{1}$$

ICCS Camera Ready Version 2026
To cite this paper please use the final published version:
DOI: 10.1007/978-3-032-29909-3_30

where $I(x, y)$ is the ideal sharp image, $d_x(\lambda)$, $d_y(\lambda)$ represent lateral displacements for each wavelength λ, and x and y are pixel coordinates.

The axial (longitudinal) CA, causing color-dependent defocus along the optical axis, can be defined as follows:

$$\mathrm{CA}_{\mathrm{axial}}(z) = \Delta z \cdot \left(\frac{\lambda_b - \lambda_r}{\lambda_g - \lambda_r} \right), \tag{2}$$

with Δz denoting the focal plane shift. The lateral (transverse) CA manifests as color fringing, increasing radially from the optical center:

$$\mathrm{CA}_{\mathrm{lateral}}(r) = k \cdot r \cdot \left(\frac{1}{f(\lambda_b)} - \frac{1}{f(\lambda_r)} \right), \tag{3}$$

where r is the radial distance, $f(\lambda)$ the focal length for wavelength λ, and k a lens-specific constant. These distortions produce characteristic purple or green fringes along high-contrast edges. The proposed method targets these spectral misalignments directly through a hybrid architecture that combines global context modeling with channel-aware processing, enabling precise detection and localization of such artifacts in real-world photographs.

Chromatic aberration identification task The task of CA identification can be formally defined as a pixel-wise binary segmentation problem aimed at detecting regions affected by wavelength-dependent optical distortions in a color image. Given an input RGB image $\mathbf{I} \in \mathbb{R}^{H \times W \times 3}$, the goal is to produce a probability map $\mathbf{M} \in [0, 1]^{H \times W}$ where each pixel value indicates the likelihood of CA presence.

Formally, the identification task is to learn a mapping $f_\theta : \mathbf{I} \to \mathbf{M}$ parameterized by θ, such that $\mathbf{M}(i, j) \approx 1$ if pixel (i, j) exhibits significant inter-channel misalignment consistent with the above models, and $\mathbf{M}(i, j) \approx 0$ otherwise.

3.2 Formal definition of the proposed architecture

The proposed ViT-SpSH model can be formally defined as follows. Given an input RGB image $\mathbf{I} \in \mathbb{R}^{H \times W \times 3}$, the pretrained ViT encoder first divides the image into non-overlapping patches of size $P = 16$ and processes them through multiple transformer layers, producing a sequence of enriched patch embeddings $\mathbf{E} \in \mathbb{R}^{N \times D}$ (where $N = HW/P^2$ and D is the embedding dimension). These embeddings capture long-range spatial dependencies via multi-head self-attention, providing robust global context essential for identifying subtle color misalignments across the entire scene.

To explicitly model the spectral characteristics of CA, manifesting as wavelength-dependent channel shifts, the SpSH computes chromatic residual maps:

$$\mathbf{R}_{rg}, \mathbf{R}_{gb}, \mathbf{R}_{rb} \in \mathbb{R}^{H \times W}$$

as absolute pairwise differences between the normalized RGB channels:

$$\mathbf{R}_{ij}(x, y) = \left| \mathbf{I}_{ij}(x, y) \right|, \quad ij \in \{rg, gb, rb\}.$$

ICCS Camera Ready Version 2026
To cite this paper please use the final published version:
DOI: 10.1007/978-3-032-29909-3_30

These residuals are projected into the ViT embedding space and fused with the patch embeddings $\mathbf{E}$ through cross-attention layers, allowing dynamic emphasis on regions exhibiting significant inter-channel discrepancies. The fused features are subsequently upsampled via a lightweight convolutional decoder consisting of transposed convolutions and residual connections, yielding a high-resolution probability map $\mathbf{M} \in [0,1]^{H \times W}$ that precisely delineates chromatic fringe locations.

4 Experimental results

In this section, the performance of the proposed ViT-SpSH model is quantitatively and qualitatively compared against several baselines on the task of CA detection. The following reference models are evaluated: a classical convolutional neural network (CNN), a lightweight U-Net, and a fully convolutional network based on pretrained VGG16 (FCN-VGG). All models are trained on the same dataset, ensuring a systematic comparison.

4.1 Preliminaries and setup

Dataset The experiments utilized a set of real-world photographs, coming from the IMAGINE dataset [3], classified into two categories: images displaying evident chromatic aberration (class: CA) and images without CA (class: no CA). This dataset comprises around 800 images, with a minimum of 400 examples in each class, encompassing diverse scenarios, illumination settings, and degrees of aberration severity to facilitate a robust and practical assessment of the proposed approach.

Meta parameters and implementation The ViT-SpSH model was trained using an early stop mechanism (ESM) with an initial number of epochs set to 100. The ESM stopped the training when the loss stopped decreasing for at least 10 epochs. The learning rate was set to 0.001, and the Adam optimizer was used.

The experiments were held on a Gigabyte Aero notebook equipped with an Intel Core i7-13700H CPU with 32 gigabytes of RAM and an Nvidia GeForce RTX 4070 GPU with 8 gigabytes of video memory. Scripts were implemented under the PyTorch framework (with Nvidia CUDA support).

Evaluation metrics To evaluate the performance of the proposed method and the baselines in the binary classification task (CA vs. no CA), standard metrics are used, including accuracy, precision, recall, and F_1-score (we do not recall their formulas due to paper limitations). The results are reported per class as well as in terms of macro-averaged scores. Since the classes are approximately balanced, macro-averaged precision, recall, and F_1-score are computed as the unweighted mean of the corresponding per-class metrics, ensuring equal contribution from both classes.

ICCS Camera Ready Version 2026
To cite this paper please use the final published version:
DOI: 10.1007/978-3-032-29909-3_30

For a graphic visualization, we use the ROC (receiver operating characteristic) curve, which is the plot of the true positive rate (TPR) against the false positive rate (FPR). The AUC (area under curve) measure describes the efficacy of the classifier. The AUC closer to 1, the better the classification accuracy, if the AUC is equal to 0.5, then a classifier gives the accuracy equal to a random division.

4.2 Baseline models

Let us recall the baseline models used in this study.

Classic CNN We consider a convolutional neural network (further denoted as classic CNN) consisting of three convolutional layers with increasing channel depth ($64 \rightarrow 128 \rightarrow 256$), each followed by max-pooling and SELU [11] activation, and a single linear layer producing the final class prediction [12].

U-Net The U-Net baseline serves as a convolutional reference for CA segmentation. It employs a symmetric encoder-decoder structure with skip connections that preserve high-resolution features from early layers while progressively downsampling and upsampling the feature maps. The encoder consists of repeated double-convolution blocks followed by max-pooling, capturing multi-scale contextual information, whereas the decoder uses transposed convolutions to recover spatial details.

FCN-VGG The FCN-VGG baseline adapts the fully convolutional network paradigm using a pretrained VGG16 backbone as the feature extractor. The convolutional layers of VGG16 progressively reduce spatial resolution while increasing channel depth, culminating in rich semantic features at the deepest stage. A 1×1 scoring convolution reduces the channel dimension to produce class predictions, which are then upsampled to the original resolution via bilinear interpolation. The approach is computationally efficient and capable of capturing hierarchical features.

4.3 Experimental results

Visual inspection of CA detection A visualization of the CA detection can be seen in Fig. 2 and 3.

Figures 2 and 3 illustrate the qualitative localization of CA using the proposed ViT-SpSH method on a representative input image. The top panel depicts the original image with visible color fringing along high-contrast edges, such as tree branches. The bottom panel shows the generated CA heatmap, where red-orange hues highlight regions of elevated aberration intensity on a normalized 0–1 scale. This visualization underscores the method's sub-pixel precision in identifying CA hotspots, with the option to partition the image into a 3×3 grid (or alternative schemes) for more targeted localization of affected regions, enabling efficient post-processing corrections.

ICCS Camera Ready Version 2026
To cite this paper please use the final published version:
DOI: 10.1007/978-3-032-29909-3_30

Fig. 2. Input image (top) showing visible chromatic aberration along object edges (i.a. tree branches); Corresponding heatmap (bottom) of detected CA, where red-orange regions highlight areas of high aberration intensity (scale: 0–1, normalized).

ICCS Camera Ready Version 2026
To cite this paper please use the final published version:
DOI: 10.1007/978-3-032-29909-3_30

Fig. 3. Input image (top) showing visible chromatic aberration along object edges; Corresponding heatmap (bottom) of detected CA, where red-orange regions highlight areas of high aberration intensity (scale: 0–1, normalized).

ICCS Camera Ready Version 2026
To cite this paper please use the final published version:
DOI: 10.1007/978-3-032-29909-3_30

Analysis of metrics The comparison metrics of CA detection are presented in Tab. 1 and 2.

Table 1. Comparison of classification performance for CA detection across different methods.

Method	Class	Precision	Recall	F_1
ViT-SpSH	no CA	0.96	0.97	0.97
	CA	0.97	0.96	0.96
Classic CNN	no CA	0.73	0.74	0.74
	CA	0.74	0.73	0.73
U-Net	no CA	0.85	0.87	0.86
	CA	0.87	0.85	0.86
FCN-VGG	no CA	0.89	0.90	0.90
	CA	0.90	0.89	0.89

The results presented in the table demonstrate the superior performance of the proposed model. The ViT-SpSH achieves precision, recall, and F_1-scores of approximately 0.96-0.97 on both classes (CA and no CA), which significantly outperforms the baselines. The classic CNN obtains the weakest results, with F_1-scores around 0.73–0.74, indicating substantial difficulties in distinguishing subtle color fringing from other edge artifacts. The U-Net performs moderately better (F_1 about 0.86), while FCN-VGG approaches closer to the proposed method (F_1 about 0.90). Overall, the consistent high scores of the proposed approach highlight the effectiveness of integrating global contextual modeling with spectrum-aware processing, resulting in robust and reliable CA identification even in challenging real-world images.

Table 2. Macro-averaged classification performance for chromatic aberration detection.

Method	Accuracy	$\mathrm{P}^{\mathrm{macro}}$	$\mathrm{R}^{\mathrm{macro}}$	F_1^{macro}
ViT-SpSH	0.96	0.97	0.97	0.97
Classic CNN	0.74	0.74	0.74	0.74
U-Net	0.86	0.86	0.86	0.86
FCN-VGG	0.90	0.90	0.90	0.90

The results summarized in the table also highlight the advantage of the proposed method. The ViT-SpSH obtains an overall accuracy of 0.96-0.97 and macro-averaged precision, recall, and F_1-score, which demonstrates its near-perfect balanced performance across both classes. In contrast, the classic CNN baseline achieves the lowest scores (0.74 for all measures). The U-Net serves better (all measures of 0.86), while FCN-VGG performs strongest among the baselines for all considered measures (0.90). Therefore, the proposed approach outperforms all baseline models, underscoring the benefits of transformer-based

ICCS Camera Ready Version 2026
To cite this paper please use the final published version:
DOI: 10.1007/978-3-032-29909-3_30

ViT-SpSH

	no CA	CA
no CA	97.0	3.0
CA	4.0	96.0

Classic CNN

	no CA	CA
no CA	74.0	26.0
CA	27.0	73.0

U-Net

	no CA	CA
no CA	87.0	13.0
CA	15.0	85.0

FCN-VGG

	no CA	CA
no CA	90.0	10.0
CA	11.0	89.0

Fig. 4. Confusion matrices (in percentages) for binary classification of images with (CA) and without (no CA) chromatic aberration.

global context modeling combined with spectral-aware mechanisms for robust CA detection. The Fig. 4 presents the confusion matrices for CA detection.

The confusion matrices in the figure again illustrate the superior classification performance of the ViT-SpSH method compared to baselines. The proposed method exhibits a nearly diagonal matrix with only minimal off-diagonal errors (3% false positives and 4% false negatives), achieving outstanding separation between the CA and no CA classes. In contrast, the classic CNN shows significant confusion, with 26–27% misclassification rates in both directions, reflecting its difficulty in capturing subtle spectral distortions. U-Net performs better, with 13–15% errors, benefiting from skip connections that aid in preserving edge details, while FCN-VGG further improves to 10–11% errors. Nonetheless, the proposed approach demonstrates markedly lower confusion, underscoring the efficacy of attention mechanisms combined with spectrum-aware processing in reliably distinguishing chromatic fringes from other visual artifacts.

The ROC curves for CA detection for all considered models are presented in Fig. 5.

The proposed ViT-SpSH model obtained the best results in terms of the AUC measure, which was equal to 0.94. The baseline methods achieved lower values, resulting in AUC equal to 0.74 for the classic CNN, 0.83 for U-Net, and 0.87 for FCN-VGG. This confirms the reliability of the discussed model among other approaches.

5 Conclusion

In this work, we presented a hybrid ViT-SpSH architecture tailored for the detection and precise localization of chromatic aberration in real-world images. The method integrated a pretrained visual transformer (ViT) encoder for global contextual modeling with a dedicated spectral segmentation head (SpSH) that explicitly processed chromatic residual maps through early feature fusion and cross-attention refinement. The proposed method effectively captured both long-range spatial dependencies and wavelength-specific misalignments. The model was trained on real-world photographic images, and extensive experiments demonstrated that the hybrid design significantly outperforms classical baselines, in-

ICCS Camera Ready Version 2026
To cite this paper please use the final published version:
DOI: 10.1007/978-3-032-29909-3_30

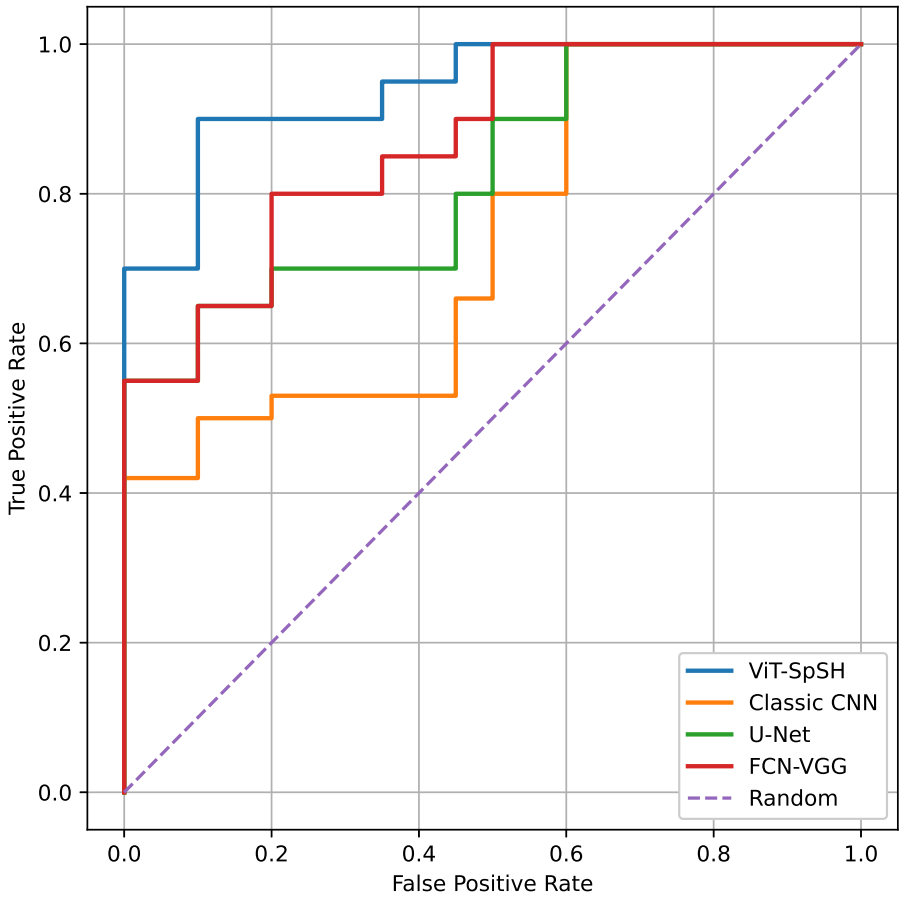

Fig. 5. ROC curves for the proposed and baseline models for CA detection.

ICCS Camera Ready Version 2026
To cite this paper please use the final published version:
DOI: 10.1007/978-3-032-29909-3_30

cluding CNN, U-Net, and FCN-VGG in binary classification accuracy in terms of accuracy, precision,m recall, and F_1 measures.

Future work could explore extensions to video sequences by utilizing temporal consistency, integration with aberration correction pipelines, or adaptation to other optical artifacts such as distortion or vignetting. Overall, the hybrid approach highlights the potential of combining transformer-based global reasoning with domain-specific spectral processing to address challenging problems in computational photography.

References

1. Akbari, Y., Al-Máadeed, S., Elharrouss, O., Khelifi, F., Lawgaly, A., Bouridane, A.: Digital forensic analysis for source video identification: A survey. Forensic Science International: Digital Investigation **41**, 301390 (2022)
2. Bernacki, J.: Digital camera identification based on analysis of optical defects. Multimedia Tools and Applications **79**(3), 2945–2963 (2020)
3. Bernacki, J., Scherer, R.: Imagine dataset: Digital camera identification image benchmarking dataset. In: SECRYPT. pp. 799–804 (2023)
4. Bimurzaev, S., Sautbekova, Z.: Transmission electron microscope with a mirror objective free of spherical and axial chromatic aberrations. Ultramicroscopy p. 114168 (2025)
5. Chan, J., Zhao, X., Zhong, S., Zhang, T., Fan, B.: Chromatic aberration correction in harmonic diffractive lenses based on compressed sensing encoding imaging. Sensors **24**(8), 2471 (2024)
6. Chen, C., Cai, X., Yi, B., Chang, Q., Luo, H., Chen, X.: Compensation of the transverse chromatic aberration in a color-coded fringe projection profilometry. Applied Optics **64**(18), 4949–4955 (2025)
7. Garfinkel, S.L.: Digital forensics research: The next 10 years. digital investigation **7**, S64–S73 (2010)
8. Gawne, T.J., Banks, M.S.: The role of chromatic aberration in vision. Annual Review of Vision Science **10** (2024)
9. Hawkes, P.: Aberration correction past and present. Philosophical Transactions of the Royal Society A: Mathematical, Physical and Engineering Sciences **367**(1903), 3637–3664 (2009)
10. Kordecki, A., Palus, H., Bal, A.: Practical vignetting correction method for digital camera with measurement of surface luminance distribution. Signal, Image and Video Processing **10**(8), 1417–1424 (2016)
11. Kılıçarslan, S., Adem, K., Çelik, M.: An overview of the activation functions used in deep learning algorithms. Journal of New Results in Science **10**(3), 75–88 (2021). https://doi.org/10.54187/jnrs.1011739
12. Li, Z., Liu, F., Yang, W., Peng, S., Zhou, J.: A survey of convolutional neural networks: Analysis, applications, and prospects. IEEE Transactions on Neural Networks and Learning Systems **33**(12), 6999–7019 (2022). https://doi.org/10.1109/TNNLS.2021.3084827
13. Lin, X., Wang, S., Deng, J., Fu, Y., Bai, X., Chen, X., Qu, X., Tang, W.: Image manipulation detection by multiple tampering traces and edge artifact enhancement. Pattern Recognition **133**, 109026 (2023). https://doi.org/https://doi.org/10.1016/j.patcog.2022.109026, https://www.sciencedirect.com/science/article/pii/S0031320322005064

ICCS Camera Ready Version 2026
To cite this paper please use the final published version:
DOI: 10.1007/978-3-032-29909-3_30

14. Liu, H., Liu, J., Zhou, W., Xu, B., Xiong, D., Yang, X.: Impact of axial chromatic aberration on color-multiplexed differential phase contrast microscopy: A quantitative study. Optics and Lasers in Engineering **184**, 108660 (2025)
15. Liu, Y., Yang, Z.H., Yu, Y.J., Wu, L.A., Song, M.Y., Zhao, Z.H.: Chromatic-aberration-corrected hyperspectral single-pixel imaging. In: Photonics. vol. 10, p. 7. MDPI (2022)
16. Lukas, J., Fridrich, J., Goljan, M.: Determining digital image origin using sensor imperfections. In: Image and Video Communications and Processing 2005. vol. 5685, pp. 249–260. SPIE (2005)
17. Lukas, J., Fridrich, J., Goljan, M.: Digital camera identification from sensor pattern noise. IEEE Transactions on Information Forensics and Security **1**(2), 205–214 (2006)
18. Manion, G.N., Stokkermans, T.J.: Chromatic aberration. In: StatPearls [Internet]. StatPearls Publishing (2023)
19. Mayer, O., Stamm, M.: Improved forgery detection with lateral chromatic aberration. In: 2016 IEEE International Conference on Acoustics, Speech and Signal Processing (ICASSP). pp. 2024–2028. IEEE (2016)
20. Mayer, O., Stamm, M.C.: Accurate and efficient image forgery detection using lateral chromatic aberration. IEEE Transactions on information forensics and security **13**(7), 1762–1777 (2018)
21. Mehrjardi, F.Z., Latif, A.M., Zarchi, M.S., Sheikhpour, R.: A survey on deep learning-based image forgery detection. Pattern Recognition **144**, 109778 (2023)
22. Mihaila, M.C.C., Laštovičková Streshkova, N., Kozák, M.: Light-based chromatic aberration correction of ultrafast electron microscopes. Physical Review Letters **134**(20), 203802 (2025)
23. Rayas, J., Sicardi-Segade, A., Martínez-García, A.: Chromatic aberration compensation of a lens for use in any ccd camera. Experimental Mechanics pp. 1–14 (2025)
24. Ricolfe-Viala, C., Sanchez-Salmeron, A.J.: Lens distortion models evaluation. Applied optics **49**(30), 5914–5928 (2010)
25. Rodriguez-Lopez, V., Dotor-Goytia, P., Moreno, E., Vinas-Pena, M.: Differences in perceived chromatic aberration between emmetropic and myopic eyes using adaptive optics. Frontiers in Medicine **12**, 1504560 (2025)
26. Schmidt, K., Guo, N., Wang, W., Czarske, J., Koukourakis, N.: Chromatic aberration correction employing reinforcement learning. Optics Express **31**(10), 16133–16147 (2023)
27. Wu, J., Li, D., Cui, A., Gao, J., Zhou, K., Liu, B.: Digital infrared chromatic aberration correction algorithm for a membrane diffractive lens based on coherent imaging. Applied Optics **61**(34), 10080–10085 (2022)
28. Xiong, J., Wang, Z., Shan, Y., Cheng, D., Wang, Y.: Eliminating chromatic aberrations of diffractive lenses in varifocal virtual reality displays. Photonics Research **13**(12), 3466–3475 (2025)
29. Yerushalmy, I., Hel-Or, H.: Digital image forgery detection based on lens and sensor aberration. International journal of computer vision **92**(1), 71–91 (2011)
30. Yu, S., Yang, H., Cui, H., Wu, Y., Cao, H.: A multi-task learning framework for textureaware chromatic aberration detection. In: 2024 Asia-Pacific Conference on Image Processing, Electronics and Computers (IPEC). pp. 206–213. IEEE (2024)
31. Zhang, J.: Visual content authenticity detection and deep forged image recognition. In: 2024 5th International Conference on Computer Vision, Image and Deep Learning (CVIDL). pp. 186–189. IEEE (2024)

ICCS Camera Ready Version 2026
To cite this paper please use the final published version:
DOI: 10.1007/978-3-032-29909-3_30